ACS APPLIED MATERIALS & INTERFACES

Research Article

www.acsami.org

Highly Magneto-Responsive Elastomeric Films Created by a Two-Step Fabrication Process

Sophie Marchi,*[,†] Alberto Casu,[‡,⊥] Franco Bertora,[§] Athanassia Athanassiou,[†] and Despina Fragouli*[,†]

[†]Smart Materials, Nanophysics, Istituto Italiano di Tecnologia, Via Morego 30, 16163 Genova, Italy

[‡]Nanochemistry, Istituto Italiano di Tecnologia, Via Morego 30, 16163 Genova, Italy

[§]Robotics Brain and Cognitive Science, Istituto Italiano di Tecnologia, Via Morego 30, 16163 Genova, Italy

[⊥]Biological and Environmental Sciences and Engineering Division, King Abdullah University for Science and Technology, Thuwal 23955-6900, Kingdom of Saudi Arabia

Supporting Information

ABSTRACT: An innovative method for the preparation of elastomeric magnetic films with increased magneto-responsivity is presented. Polymeric films containing aligned magnetic microchains throughout their thickness are formed upon the magnetophoretic transport and assembly of microparticles during polymer curing. The obtained films are subsequently magnetized at a high magnetic field of 3 T directed parallel to the orientation of the microchains. We prove that the combination of both alignment of the particles along a favorable direction during curing and the subsequent magnetization of the solid films induces an impressive increase of the films' deflection. Specifically, the displacements reach few millimeters, up to 85 times higher than those of the nontreated films with the same particle concentration. Such a process can improve the performance of the magnetic films without increasing the amount of magnetic fillers and, thus, without compromising the mechanical properties of the resulting composites. The proposed method can be used for the fabrication of magnetic films suitable as components in systems in which large displacements at relatively low magnetic fields are required, such as sensors and drug delivery or microfluidic systems, especially where remote control of valves is requested to achieve appropriate flow and mixing of liquids.

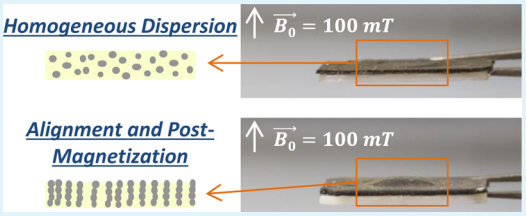

KEYWORDS: *PDMS, microparticles, magnetic assembly, ferromagnetism, magnetic actuation*

1. INTRODUCTION

Polymeric membrane actuators have been extensively employed as components in diverse technological systems such as micropumps, or valves in microfluidic devices.[1−15] For these purposes, various actuation principles have been adopted, including electrostatic,[2,3,6] thermal,[4,14] or piezoelectric.[1,7] However, these methods present diverse limitations, making their direct utilization in the final devices difficult. In particular, in the case of electrostatic actuation, a high driving voltage is generally required,[16,17] while the response of thermally actuated membranes is usually slow.[18] Lastly, in many cases, piezoelectric polymeric films exhibit a creep effect,[19] meaning that the material continues to expand even after the removal of the actuation stimulus, prohibiting thus the immediate return to its initial state.

The magnetic actuation results in an interesting alternative to the principles mentioned above, because of the lack of electrical connections, the possibility of being manipulated at a large distance, and the fast response to the external magnetic field.[9,11,13] The first magnetic polymeric actuators, made from a mixture of magnetic particles with rigid polymeric matrices, were mainly used as permanent magnets, magnetic cores, or connecting elements.[20] These classical actuators presented low flexibility, and their size or shape remained unaffected under the effect of the magnetic field, limiting their range of applications.

Alternatively, the new generation of magnetic elastomers, which consists of magnetic nano- or microparticles (such as iron, Fe_3O_4, or carbonyl iron) dispersed in highly elastic polymeric matrices, can achieve large and nonhomogeneous deformation together with a fast response to an external magnetic field.[11,12,21−25] Therefore, this class of magnetic materials opened new opportunities for their utilization in various applications where soft actuators are required such as microfluidic systems or micropumps.[12,21] Indeed, the low elastic modulus of the polymeric matrix allows a direct transfer to the polymeric chains of the forces acting on the magnetic particles under the external field, thus resulting in rapid actuation of flat membranes. However, to obtain high deflection values, relatively high magnetic fields should be applied (e.g., under an external magnetic field of 417 mT, a deflection of 125 μm is observed for a film 4 mm in diameter)[11] or large diameters should be employed (e.g., 125 μm deflection under an 18 mT magnetic field for a film 50 mm in diameter).[26] This

Received: May 29, 2015
Accepted: August 3, 2015
Published: August 24, 2015

DOI: 10.1021/acsami.5b04711
ACS Appl. Mater. Interfaces 2015, 7, 19112−19118

phenomenon is the main drawback for their direct utilization in many applications.

One possibility of strengthening the magnetic response, and therefore the deflection of these systems in lower fields, is the use of higher-performance magnetic particles, such as the anisotropic rare earth ferromagnetic powders like $Nd_2Fe_{14}B$ alloys.[9,27] Such microparticles present exceptional magnetic properties[27,28] and can be permanently magnetized. Alternatively, the magnetic response of the polymeric magnetic films can be sufficiently improved by arranging the particles in a preferential direction throughout the volume of the polymeric matrix. In this way, the magnetic properties of the films become anisotropic. Previous works have evidenced the possibility of aligning magnetic particles within thin plastic films by magnetophoretic transport and assembly of the dispersed magnetic particles.[29−34] The dimensions of the wires are strictly dependent on the strength of the applied magnetic field, the duration of its application, and the curing or evaporation rate of the solvent if it is present. Their magnetization has a strong anisotropy with a higher value toward the direction of the assembled chains,[29,30,32] allowing the formation of functional magnetic films.

However, to the best of our knowledge, only few studies point to the deflection enhancement of polymeric films due to the magnetophoretic transport and assembly of magnetic particles in a polymer film.[35] Most importantly, the combination of the alignment of anisotropic ferromagnetic particles in a polymeric film and the subsequent magnetization of the solid composite results in an interesting way of greatly increasing the magneto-responsivity of the films. Therefore, herein, we report the preparation of highly magneto-responsive elastomeric composite films by using microparticles of a $Nd_2Fe_{14}B$ alloy as fillers assembled preferentially in a defined direction. We show that the magnetophoretic transport and assembly of the particles, which results in the formation of microchains of assembled particles throughout the volume of the film, in combination with the subsequent magnetization of the solid composite lead to an impressive increase of the film's deflection. Specifically, under low magnetic fields, the values are up to 85 times higher than those of nontreated composites with the same content of particles. Therefore, such a type of process improves the performance of the magnetic films without increasing the amount of magnetic fillers in the polymer matrix, which is kept to relatively low concentrations to preserve the pristine mechanical characteristics of the elastomeric matrix.

2. EXPERIMENTAL SECTION

2.1. Materials. The silicon elastomer Ecoflex 10 from Smooth-on was used as received. It consists of two components: a base and a curing agent (1:1 mixing ratio). Anisotropic ferromagnetic particles MQA-36-18 based on a $Nd_2Fe_{14}B$ alloy (PrNdFeCoBDyGa) with an average size (D_{50}) of <105 μm were kindly provided by Magnequench GmbH (Molycorp Co.). The magnetic properties of the particles were as follows: remanence, B_r = 1240 mT; intrinsic coercivity, H_{ci} = 18.0 kOe; and energy product, $(BH)_{max}$ = 36 MGOe. The morphology of the particles and their composition are presented in Figure S1 of the Supporting Information.

2.2. Sample Preparation. The magnetic particles were manually mixed with the base (10−50 wt % with respect to the final composite) and sonicated with an ultrasonic bath for few minutes at 59 kHz to obtain the optimal dispersion. Subsequently, the curing agent was added (1:1 base:curing agent weight ratio), and after being manually mixed for few seconds, the final solution was poured onto a Teflon substrate, spin-coated at 500 rpm for 30 s, and left to cure at room temperature for 3 h. During curing, some of the films were subjected to a homogeneous external magnetic field of 200 mT produced by a cylindrical neodymium static magnet (diameter D of 25 mm, thickness t of 10 mm) and directed along the normal to the surface of the films. To achieve a complete curing, the samples were subsequently put in an oven at 80 °C overnight. The resulting films (thickness of 400 μm) were then released from the Teflon mold and glued with silicone sealant (Elastosil, Wacher Chemie AG) on an epoxy substrate with a 10 mm central hole to allow the deflection of the free part of the film.

Following the procedure mentioned above, four different types of films were prepared: (a) films with magnetic particles distributed homogeneously in the whole volume of the polymer (S_H samples), (b) films with magnetic particles whose easy axis is oriented preferentially in a direction normal to the surface, forming magnetic microchains throughout the polymer matrix (S_A samples) (this type is obtained upon application of an external magnetic field of 200 mT, as previously described), (c) S_A films subsequently magnetized in a 3 T magnetic field, higher than the coercivity of the particles ($S_{Apost3T}$ samples), and (d) S_H films magnetized in a 3 T magnetic field ($S_{Hpost3T}$).

The 3 T magnetization field was generated by an MRI Scanner (3 T Excite HDx GE Medical Systems): the magnetizing field direction was parallel to the aligning direction of the particles to achieve a synergistic effect. The samples were left under the 3 T magnetic field for 15 s.

2.3. Characterization. *2.3.1. Morphological Analysis.* A stereomicroscope in transmission mode (Leica S8 APO) equipped with a digital camera accessory and image processing software was used to image the surface and the cross section of the magnetic films prepared according to the different, previously stated, methods.

Scanning electron microscopy (SEM) imaging was performed with a JEOL JSM-6490LA instrument (Jeol-Japan), equipped with a tungsten thermionic electron source operated at an acceleration voltage of 15 kV. Samples were prepared via freeze fracture in liquid nitrogen to expose the cross section. The imaging for the S_A and S_H samples was performed using the backscattered electron detector to have compositional contrast and to enhance the difference between the $Nd_2Fe_{14}B$ particles and the elastomeric matrix. Because of the nonconductive nature of the polymer, the low-vacuum mode (25 Pa) was adopted to avoid metallic coating, which could have masked the compositional contrast.

2.3.2. Deflection Measurements. The deflection was measured using a laser optical sensor ILD 2200 (from Micro-Epsilon), and the scheme of the experimental setup is reported in Figure S2 of the Supporting Information. The magnetic films, previously fixed on an epoxy substrate with a central hole 10 mm in diameter, deflect in a direction normal to their surface under the effect of an external magnetic field generated by a cylindrical neodymium static magnet (diameter D of 25 mm, thickness t of 10 mm), and the sensor records the deflection value. The strength of the field is modified by varying the distance between the magnet and the film (Figure S3 of the Supporting Information). The measurements were conducted three times on two different samples for each composition.

2.3.3. Magnetic Characterization Measurements. Measurements of static magnetization and hysteresis loops were performed on a Quantum Design MPMS SQUID (Superconducting Quantum Interference Device) magnetometer, equipped with a superconducting magnet capable of producing fields up to 7 T. Hysteresis loops were recorded at room temperature with a maximal applied field of ±3 T. The applied field was normal to the surface of the films, so that its direction was parallel to the magnetic fields previously used during the alignment and magnetization procedures. The data were normalized with respect to the precise mass of the particles within the samples as defined by thermogravimetric analyses (TGA Q500-TA Instruments). Specifically, the samples used for the magnetic measurements and a pure elastomer sample were heated to 900 °C at a rate of 10 °C min^{-1} in air (flow rate of 50 mL min^{-1}), to degrade all the organic components. The residual mass obtained at the end of the experiment for each composite sample was compared with the residual mass obtained for the pure polymer to calculate the exact amount of magnetic content inside each film.

DOI: 10.1021/acsami.5b04711
ACS Appl. Mater. Interfaces 2015, 7, 19112−19118

3. RESULTS AND DISCUSSION

To evaluate the appropriate magnetic content of the composite films that leads to the highest magneto-responsivity, deflection measurements were first conducted on the S_H composites loaded with up to 50 wt % magnetic particles (Figure 1). The

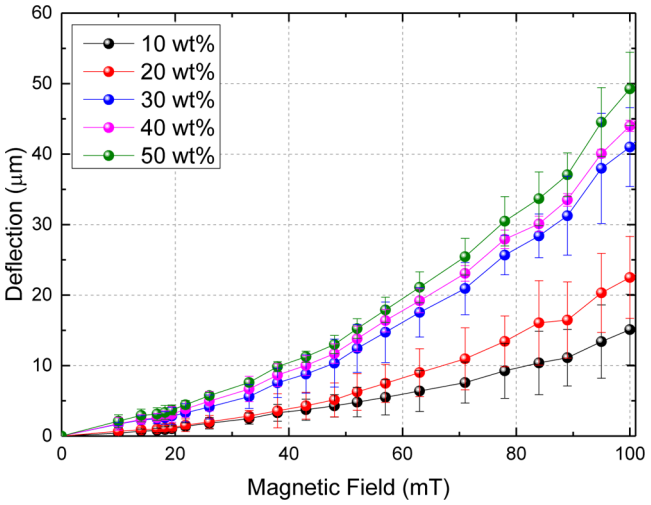

Figure 1. Deflections at different applied magnetic fields for S_H films with different concentrations of particles.

displacement values increase with the increase in particle concentration. In particular, the maximal displacement achieved under an external magnetic field of 100 mT is 41 μm for the 30 wt % S_H sample, 86% higher than the value of 22 μm achieved for the 20 wt % S_H sample. A further increase in magnetic content does not induce any significant improvement in the deflection: the performance of the 50 wt % sample is similar to that of the 30 and 40 wt % samples. This behavior indicates that the deflection of the films is a function of not only the magnetic particle content but also the stiffness of the resulting composite film. In fact, the mechanical properties of the films are strictly dependent on both the amount of particles within the composite and its effect on the cross-linking process[36,37] (Figure S4). The progressive addition of rigid particles within a soft polymeric matrix leads to an increase in the film's stiffness that hinders its deformation upon the effect of the external field even if the magnetic content is increased.[12] Consequently, the right compromise between elastic properties and the amount of particles should be identified for the optimal performance of the composite and in this case is revealed to be 30 wt %.

To improve the deflection of the selected sample, the alignment of the particles within the elastomeric matrix is achieved by the magnetophoretic transport and assembly process under an external magnetic field. In particular, 30 wt % particles are mixed with the silicon elastomer and the curing of the composite is performed under an external magnetic field of 200 mT. This drives the particles to assemble as microchains oriented parallel to the external field's direction and perpendicular to the surfaces of the films.[29] The morphology of the cured films prepared without and with alignment of the magnetic particles, samples S_H and S_A, respectively, presents significant differences as observed by optical microscopy (Figure 2). The top view of the films shows that in the absence of alignment during curing (S_H) the magnetic particles are homogeneously dispersed in the polymer matrix, which indicates the absence of relevant interactions between the particles (Figure 2a). However, when the particles are aligned during polymer curing, they are assembled in a preferential direction forming organized features on the film's surface (Figure 2b). This is further confirmed by the investigation of the cross section of the two films (Figure 2c,d), where the formation of magnetic microchains throughout the thickness of the polymeric matrix is evidenced. This is mainly attributed to the interaction between the magnetic particles and the applied field. Specifically, during the alignment process, the polymer is not yet cured; thus, the magnetic particles can move freely in the viscous matrix under the effect of the external magnetic forces. Therefore, they tend to orient along the magnetic flux lines and to form localized microchains perpendicular to the surfaces of the films. After the end of the polymerization process, the microchains are permanently assembled into the

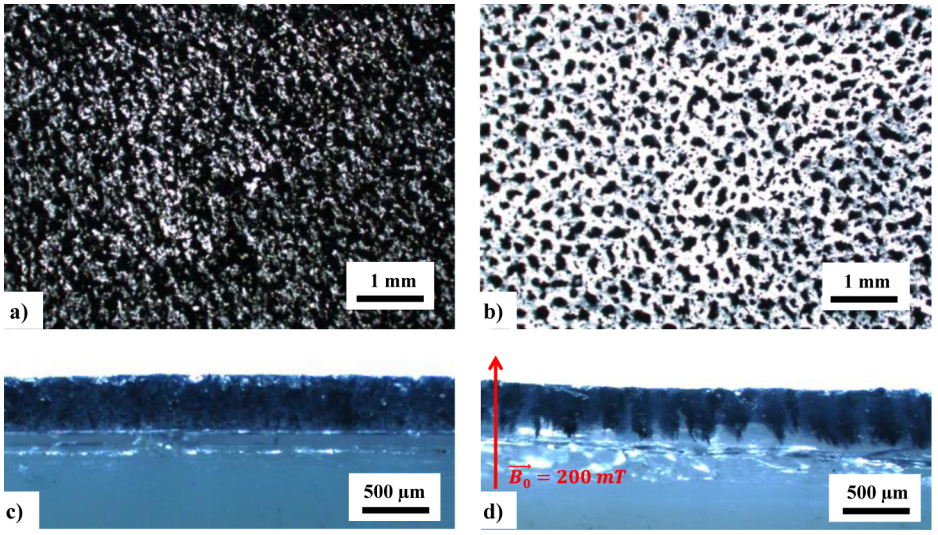

Figure 2. Optical microscopy images of magnetic films with 30 wt % magnetic particles distributed homogeneously throughout the surface and the volume of the film (a–c) or showing a preferential alignment vertically with respect to the film's surface (b–d). Top views (a and b) and cross sections (c and d).

DOI: 10.1021/acsami.5b04711
ACS Appl. Mater. Interfaces 2015, 7, 19112–19118

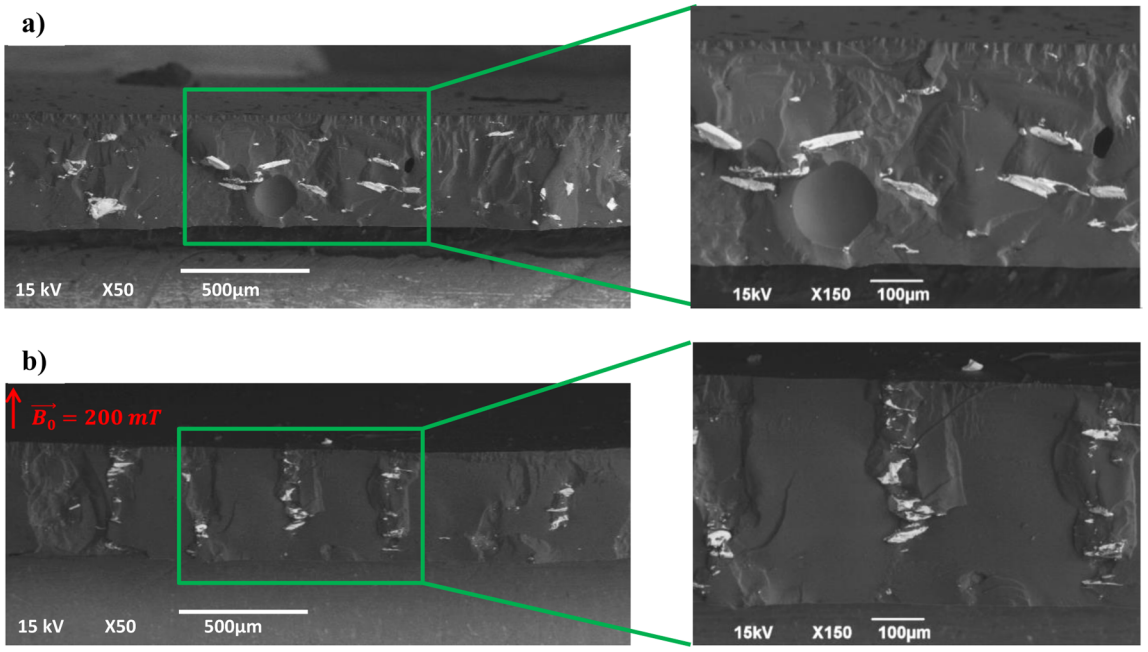

Figure 3. SEM images of (a) S_H and (b) S_A samples for both low and high magnifications. The loss of the particles along the assembled paths in panel b is attributed to the freeze fracture process.

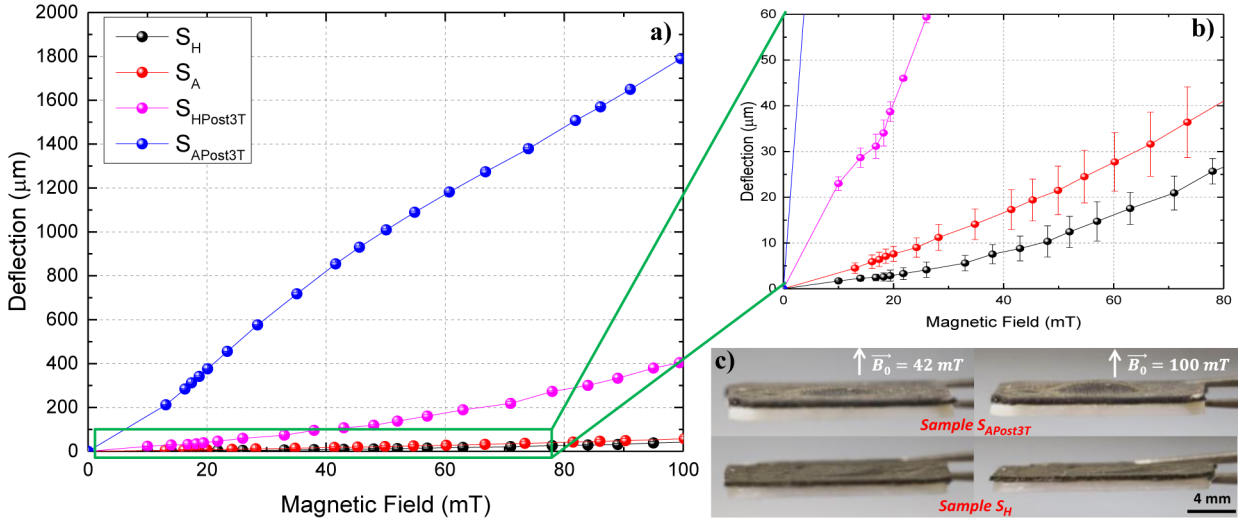

Figure 4. (a) Deflection of the films containing 30 wt % magnetic particles under different magnetic fields (the error bars are smaller than the size of the symbols). (b) Magnification in the low-deflection region. (c) Photographs of the deflection of $S_{APost3T}$ (top) and S_H (bottom) films under different magnetic fields.

elastomer matrix because of its high viscosity, which prevents any further movement of the particles.[29]

Deeper insight into the assembled microchains was achieved by SEM analysis as shown in Figure 3. In accordance with the optical microscopy study, the cross section of the S_H sample (Figure 3a) shows randomly distributed magnetic particles within the whole polymer matrix. On the contrary, as presented in Figure 3b, the particles are distributed along a preferential direction at the S_A film, and their composition is clearly shown by the EDX analysis presented in Figure S5 of the Supporting Information. The formed microchains have a mean thickness of 130 ± 35 μm, while the mean distance between them is 230 ± 40 μm.

The alignment of the particles during curing (S_A) leads to a significant increase in the deflection with respect to the S_H films as shown in Figure 4. In fact, because the magnetic field applied during the actuation is normal to the surface of the films, the magnetic microchains within the sample S_A are parallel to it and increase the magneto-responsivity of the composites. Specifically, the rough orientation of each particle's easy axis in the direction of the external field during the alignment process, in combination with their morphological arrangement in the form of microchains, results in the total increase in the magnetization of the S_A film in the specific direction.[29] This enhancement is already effective at low magnetic fields (e.g., 42 mT) with an increment of 70% of the films' response (17 μm for S_A vs 10 μm for S_H). Therefore, the significant increase in the deflection of the films after the alignment process indicates its importance for the great improvement in the magnetoresponsivity of the composite films.

DOI: 10.1021/acsami.5b04711
ACS Appl. Mater. Interfaces 2015, 7, 19112−19118

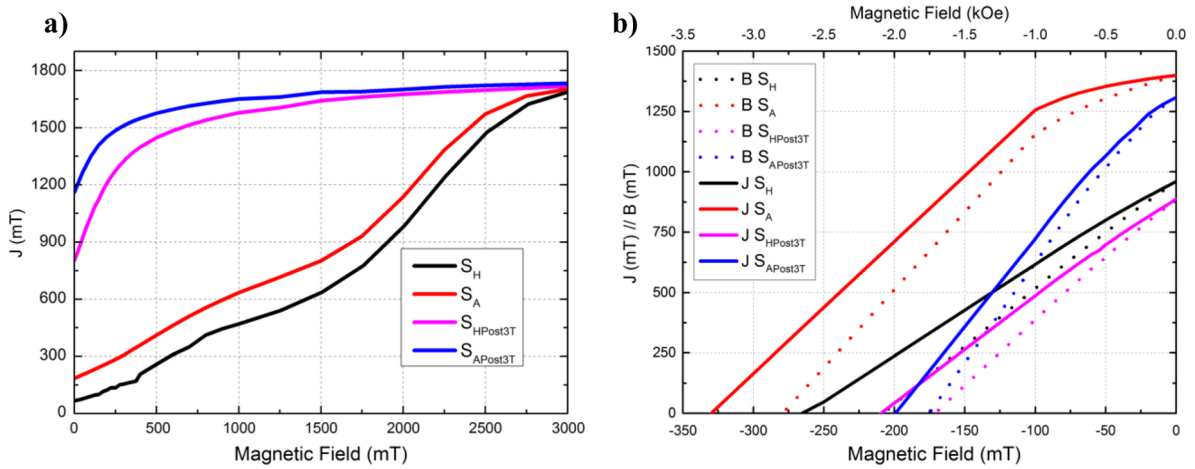

Figure 5. (a) First magnetization curves from 0 to 3 T recorded at 298 K for films containing 30 wt % magnetic particles. (b) Demagnetization curves of films containing 30 wt % magnetic particles after exposure to a 3 T external field. Solid lines indicate magnetic polarization (J), and dotted lines indicate magnetic flux density (B).

The subsequent magnetization of the S_H and S_A films is conducted at a magnetic field of 3 T, higher than the saturation magnetization of the particles (M_{sat} = 1250 mT as indicated by the supplier) with a direction normal to the surfaces of the films. As reported in Figure 4, an impressive increase in the deflection of the magnetized film ($S_{APost3T}$) is achieved with a maximal value of 1780 μm for 100 mT, while at low fields, the deflection is hundreds of micrometers, e.g., 850 μm for 42 mT, 4900% higher than the deflection recorded for the S_A film and 8400% higher than that for the S_H sample for the same actuation field. Indeed, as shown in Figure 4c, the deflection of $S_{APost3T}$ is clearly visible, even at low magnetic fields (42 mT), contrary to the deflection of the S_H sample. Interestingly, the enhancement of the magneto-responsivity due to the post-magnetization process is much more pronounced for the films in which the particles are aligned in the form of microchains compared to the films in which the particles are homogeneously dispersed, evidencing the importance of the alignment process before magnetization.

As already discussed, during the alignment process the particles assemble parallel to the external magnetic field, partially orienting their magnetic moment in that preferential direction and inducing a synergistic effect for the final magnetic moment of the assembled microchains. The subsequent magnetization of the films is a second important step for the impressive increase in the magneto-responsivity. For maximal performance the sample should be fully magnetized, and this can be achieved if the applied magnetic field for the post-treatment is higher than the one needed to attain the saturation magnetization of the particles. Indeed, magnetization performed with a lower magnetic field (500 mT) showed that the post-treatment was not sufficient to reach similar deflections with the $S_{APost3T}$ film (Figure S6 of the Supporting Information). Therefore, during the $S_{APost3T}$ film magnetization, the size of the magnetic domains is maximized as each magnetic particle reaches its saturation state, resulting in a subsequent increase in the total magnetic moment of the whole microchain of which it is a component. In fact, the application of a high magnetic field promotes the increase in the residual magnetization of the ferromagnetic particles, which results in a responsivity higher than those of the pristine ones. In this way, the total magnetic moment of the microchains (in the $S_{APost3T}$ film) is a synergistic effect of the magnetic moments of the individual particles, while the magnetizing field in the post-treatment provokes their complete rotation toward their preferential direction. This leads to highly efficient films, and indeed, the deflection is much higher than those of the S_H films or to the films prepared with only one process (alignment or magnetization).

The effect of the alignment and post-magnetization procedures on the magnetic performances of the films was confirmed by analyzing their magnetic properties by collecting hysteresis loops at 298 K. The initial magnetization curves (Figure 5a) show the magnetic response of the films upon their first exposure to an increasing field going from 0 to 3 T, offering useful indications about their features. In particular, variations in the magnetization are clearly visible in the low-field region (up to 1 T), where the S_H and $S_{APost3T}$ films exhibit the lowest and highest magnetization values, respectively. The effects of the alignment and magnetization are easily recognizable, with the first determining some domain wall movements (as should be expected because of the low field applied during alignment), resulting in a slight increase in the first magnetization curve of S_A with respect to the curve of the S_H film. On the other hand, the high field applied for the post-treatment magnetization determines large irreversible jumps of the domain walls along with rotation processes, which lead to the brisk increase in the first magnetization curves of the $S_{HPost3T}$ and $S_{APost3T}$ films with respect to S_A. The combination of both treatments works as a two-step process, with the alignment being responsible for the formation of microchains of particles with magnetic domains roughly oriented along a common direction and the magnetization maximizing the size of the magnetic domains oriented along the magnetizing field.

Given the high weight percentage of magnetic species present in the polymeric matrices, interactions should play a key role in varying their magnetic parameters. The role of interactions, the formation of different-sized magnetic domains, and the overall variations occurring to the films, depending on the treatments of choice, can be studied more in detail by analyzing the residual magnetization in the absence of any external applied field (remanence B_r) and the demagnetization field (coercivity H_c) (Figure 5b and Table 1).

DOI: 10.1021/acsami.5b04711
ACS Appl. Mater. Interfaces 2015, 7, 19112−19118

Table 1. Magnetic Parameters of Parent Particles and Films

sample	magnetic particles	S_H	$S_{HPost3T}$	S_A	$S_{APost3T}$
B_r (mT)	1240	976	888	1400	1309
H_{ci} (kOe)	18.0	2.7	2.1	3.3	2.0

The B_r enhancement of the S_A and $S_{APost3T}$ films and its decrease in S_H and $S_{HPost3T}$ films with respect to the parent particles should be ascribed to the effects of the aligning process. The proximity of the particles assembled in the microchains favors exchange coupling, which in the remanent state results in the preservation of an enhanced net magnetization. On the other hand, the absence of alignment in the preparation of S_H and $S_{HPost3T}$ films determines the presence of spatially dispersed particles, so that only dipole−dipole interactions should be expected, which leads to a decreased remanence with respect to that of the parent particles. Moreover, another effect due to post-treatment magnetization can be observed with regard to the remanence of both aligned and nonaligned samples. The decrease observed in the remanence of 3 T treated samples with respect to that of the nontreated ones suggests that the formation of larger magnetic domains due to major movements of the domains walls works against maintaining the magnetic alignment of the samples in the absence of an external field.

As expected, H_{ci} values of the films are systematically smaller than those of the parent particles, because the large fraction of magnetic particles inside the films leads to interactions playing a stronger role than anisotropy in determining the magnetic features of the films. The increased alignment of grains after exposure to a 3 T external field during the hysteresis results in a strong decrease in H_{ci}, similar to what observed in $Nd_2Fe_{14}B$-sintered magnets.[9,38,39] Once again, the features of the samples vary depending on the post-magnetization process, with the $S_{HPost3T}$ and $S_{APost3T}$ samples showing the lowest H_{ci} values with respect to the S_H and S_A samples. This suggests that the increase in the size of the magnetic domains in the post-magnetization samples plays a role in further decreasing the H_{ci}.

4. CONCLUSIONS

This study clearly demonstrates the importance of both the alignment of the $Nd_2Fe_{14}B$ magnetic particles and the subsequent magnetization of the elastomeric composite in order to reach high deflection performances of films under magnetic actuation. The use of an external magnetic field for the magnetophoretic transport and assembly of the magnetic particles during the polymeric matrix's curing induces the formation of aligned magnetic microchains throughout the film's thickness. This results in an improvement in the film's deflection compared to those of the films in which particles of the same concentration are homogeneously dispersed. The subsequent magnetization of the films at a magnetic field higher than the critical field for saturation magnetization of the particles provokes an impressive increase in the deflection, with performances reaching deflection values 85 times higher than those of nontreated films, with a maximal deflection of 850 μm at 42 mT (10 μm for the S_H film), while at higher fields, e.g., 100 mT, the displacement is ∼1780 μm. Magnetic studies confirm that the alignment process is responsible for the collective effect on the magnetic moment, increasing thus the magnetic response in the direction of the microchains, while the post-magnetization process results in an enhancement of the magnetic domain sizes that are oriented along the magnetizing field. These films are suitable for applications in which high deformations at low magnetic fields are requested.

■ ASSOCIATED CONTENT

Supporting Information

The Supporting Information is available free of charge on the ACS Publications website at DOI: 10.1021/acsami.5b04711.

SEM images and EDX mapping of the magnetic particles, experimental setup for the measurements of film's deflection, magnetic field gradient used for the deflection experiments, tensile tests of the elastomeric composites, SEM images and EDX mapping of the S_A sample, and deflection measurements under diverse magnetic fields for a 500 mT post-magnetization field (PDF)

■ AUTHOR INFORMATION

Corresponding Authors

*E-mail: sophie.marchi@iit.it.
*E-mail: despina.fragouli@iit.it.

Funding

This work is financed by the EU within the BLINDPAD Project (FP7/2007-2013 Grant Agreement 611621).

Notes

The authors declare no competing financial interest.

■ ACKNOWLEDGMENTS

The magnetization at 3 T was kindly achieved by Francesca Frijia in U.O.C. Bioingegneria e ingegneria clinica (CNR-Regione Toscana) Fondazione "G. Monasterio" CNR-Regione Toscana Area della Ricerca S. Cataldo. Simone Lauciello and Alice Scarpellini from Nanochemistry and Lara Marini from Nanophysics of Istituto Italiano di Tecnologia are gratefully acknowledged for SEM/EDX and TGA analyses, respectively.

■ REFERENCES

(1) Koch, M.; Evans, A. G. R.; Brunnschweiller, A. The Dynamic Micropump Driven with a Screen Printed PZT Actuator. *J. Micromech. Microeng.* **1998**, *8*, 119−122.

(2) Chan, W. S.; Saarinen, M. J.; Talghader, J. J. Fabrication and Operation of an Electrostatic Actuator for Controlling Nanometer-Scale Gaps in Collapsed Cantilever Heterostructures. *Appl. Phys. Lett.* **2013**, *102*, 243508.

(3) Amakawa, H.; Fukuzawa, K.; Shikida, M.; Tsuji, H.; Zhang, H.; Itoh, S. An Electrostatic Actuator for Dual-Axis Micro-Mechanical Probe on Friction Force Microscope. *Sens. Actuators, A* **2012**, *175*, 94−100.

(4) Chunder, A.; Etcheverry, K.; Londe, G.; Cho, H. J.; Zhai, L. Conformal Switchable Superhydrophobic/hydrophilic Surfaces for Microscale Flow Control. *Colloids Surf., A* **2009**, *333*, 187−193.

(5) Neagu, C. R.; Gardeniers, J. G. E.; Elwenspoek, M.; Kelly, J. J. An Electrochemical Microactuator: Principle and First Results. *J. Microelectromech. Syst.* **1996**, *5*, 2−9.

(6) Tice, J. D.; Bassett, T. A.; Desai, A. V.; Apblett, C. A.; Kenis, P. J. A. A Monolithic Poly(Dimethylsiloxane) Electrostatic Actuator for Controlling Integrated Pneumatic Microsystems. *Sens. Actuators, A* **2013**, *196*, 22−29.

(7) Pabst, O.; Hölzer, S.; Beckert, E.; Perelaer, J.; Schubert, U. S.; Eberhardt, R.; Tünnermann. Inkjet Printed Micropump Actuator Based on Piezoelectric Polymers: Device Performance and Morphology Studies. *Org. Electron.* **2014**, *15*, 3306−3315.

(8) Khoo, M.; Liu, C. Micro Magnetic Silicone Elastomer Membrane Actuator. *Sens. Actuators, A* **2001**, *89*, 259−266.

DOI: 10.1021/acsami.5b04711
ACS Appl. Mater. Interfaces 2015, 7, 19112−19118

(9) Wang, W. S.; Yao, Z. M.; Chen, J. C.; Fang, J. Composite Elastic Magnet Films with Hard Magnetic Feature. *J. Micromech. Microeng.* **2004**, *14*, 1321−1327.
(10) Fahrni, F.; Prins, M. W. J.; van IJzendoorn, L. J. Magnetization and Actuation of Polymeric Microstructure with Magnetic Nanoparticles for Application in Microfluidics. *J. Magn. Magn. Mater.* **2009**, *321*, 1843−1850.
(11) Pirmoradi, F. N.; Cheng, L.; Chiao, M. A Magnetic Poly(Dimethylsiloxane) Composite Membrane Incorporated with Uniformly Dispersed, Coated Iron Oxide Nanoparticles. *J. Micromech. Microeng.* **2010**, *20*, 015032.
(12) Li, J.; Zhang, M.; Wang, L.; Li, W.; Sheng, P.; Wen, W. Design and Fabrication of Microfluidic Mixer from Carbonyl Iron-PDMS Composite Membrane. *Microfluid. Nanofluid.* **2011**, *10*, 919−925.
(13) Thévenot, J.; Oliveira, H.; Sandre, O.; Lecommandoux, S. Magnetic Responsive Polymer Composite Materials. *Chem. Soc. Rev.* **2013**, *42*, 7099−7116.
(14) Richter, A.; Klatt, S.; Paschew, G.; Klenke, C. Micropumps Operated by Swelling and Shrinking of Temperature-Sensitive Hydrogels. *Lab Chip* **2009**, *9*, 613−618.
(15) Diller, E.; Miyashita, S.; Sitti, M. Remotely Addressable Magnetic Composite Micropumps. *RSC Adv.* **2012**, *2*, 3850−3856.
(16) Tice, J. D.; Desai, A. V.; Bassett, T. A.; Apblett, C. A.; Kenis, P. J. A. Control of Pressure-Driven Components in Integrated Microfluidic Devices Using an On-Chip Electrostatic Microvalve. *RSC Adv.* **2014**, *4*, 51593−51602.
(17) Olfatnia, M.; Cui, L.; Chopra, P.; Awtar, S. Large Range Dual-Axis Micro-Stage Driven by Electrostatic Comb-Drive Actuators. *J. Micromech. Microeng.* **2013**, *23*, 105008.
(18) Zhang, X.; Pint, C. L.; Lee, M. H.; Schubert, B. E.; Jamshidi, A.; Takei, K.; Ko, H.; Gillies, A.; Bardhan, R.; Urban, J. J.; Wu, M.; Fearing, R.; Javey, A. Optically- and Thermally-Responsive Programmable Materials Based on Carbon Nanotube-Hydrogel Polymer Composites. *Nano Lett.* **2011**, *11*, 3239−3244.
(19) Changhai, R.; Lining, S. Hysteresis and Creep Compensation for Piezoelectric Actuator in Open-Loop Operation. *Sens. Actuators, A* **2005**, *122*, 124−130.
(20) Zrìnyi, M. In *Smart Polymers and Their Applications*; Aguilar, M. R., Roman, J. S., Eds.; Woodhead Publishing: Cambridge, U.K., 2014; Chapter 5, pp 134−165.
(21) Fahrni, F.; Prins, M. W. J.; van IJzendoorn, L. J. Micro-Fluidic Actuation Using Magnetic Artificial Cilia. *Lab Chip* **2009**, *9*, 3413−3421.
(22) Nanni, G.; Petroni, S.; Fragouli, D.; Amato, M.; De Vittorio, M.; Athanassiou, A. Microfabrication of Magnetically Actuated PDMS-Iron Composite Membranes. *Microelectron. Eng.* **2012**, *98*, 607−609.
(23) Abramchuk, S.; Kramarenko, E.; Stepanov, G.; Nikitin, L. V.; Filipcsei, G.; Khokhlov, A. R.; Zrìnyi, M. Novel Highly Elastic Magnetic Materials for Dampers and Seals: Part I. Preparation and Characterization of the Elastic Materials. *Polym. Adv. Technol.* **2007**, *18*, 883−890.
(24) Peng, S.; Zhang, M.; Niu, X.; Wen, W.; Sheng, P.; Liu, Z.; Shi, J. Magnetically Responsive Elastic Microspheres. *Appl. Phys. Lett.* **2008**, *92*, 012108.
(25) Abramchuk, S.; Kramarenko, E.; Grishin, D.; Stepanov, G.; Nikitin, L. V.; Filipcsei, G.; Khokhlov, A. R.; Zrìnyi, M. Novel Highly Elastic Magnetic Materials for Dampers and Seals: Part II. Material Behavior in a Magnetic Field. *Polym. Adv. Technol.* **2007**, *18*, 883−890.
(26) Singh, A.; Shirolkar, M.; Limaye, M. V.; Gokhale, S.; Khan-Malek, C.; Kulkarni, S. K. A Magnetic Nano-Composite Soft Polymeric Membrane. *Microsyst. Technol.* **2013**, *19*, 409−418.
(27) Ormerod, J.; Constantinides, S. Bonded Permanent Magnets: Current Status and Future Opportunities. *J. Appl. Phys.* **1997**, *81*, 4816−4820.
(28) Panchanathan, V. Magnequench Magnets Status Overview. *J. Mater. Eng. Perform.* **1995**, *4*, 423−429.
(29) Fragouli, D.; Buonsanti, R.; Bertoni, G.; Sangregorio, C.; Innocenti, C.; Falqui, A.; Gatteschi, D.; Cozzoli, P. D.; Athanassiou, A.; Cingolani, R. Dynamical Formation of Spatially Localized Arrays of Aligned Nanowires in Plastic Films with Magnetic Anisotropy. *ACS Nano* **2010**, *4*, 1873−1878.
(30) Lorenzo, D.; Fragouli, D.; Bertoni, G.; Innocenti, C.; Anyfantis, G. C.; Cozzoli, P. D.; Cingolani, R.; Athanassiou, A. Formation and Magnetic Manipulation of Periodically Aligned Microchains in Thin Plastic Membranes. *J. Appl. Phys.* **2012**, *112*, 083927.
(31) Fragouli, D.; Torre, B.; Villafiorita-Monteleone, F.; Kostopoulou, A.; Nanni, G.; Falqui, A.; Casu, A.; Lappas, A.; Cingolani, R.; Athanassiou, A. Nanocomposite Pattern-Mediated Magnetic Interactions for Localized Deposition of Nanomaterials. *ACS Appl. Mater. Interfaces* **2013**, *5*, 7253−7257.
(32) Fragouli, D.; Das, A.; Innocenti, C.; Guttikonda, Y.; Rahman, S.; Liu, L.; Caramia, V.; Megaridis, C. M.; Athanassiou, A. Polymeric Films with Electric and Magnetic Anisotropy Due to Magnetically Assembled Functional Nanofibers. *ACS Appl. Mater. Interfaces* **2014**, *6*, 4535−41.
(33) Ghosh, S.; Puri, I. K. Soft Polymer Magnetic Nanocomposites: Microstructure Patterning by Magnetophoretic Transport and Self-Assembly. *Soft Matter* **2013**, *9*, 2024−2029.
(34) Robbes, A. S.; Cousin, F.; Meneau, F.; Dalmas, F.; Boué, F.; Jestin, J. Nanocomposite Materials with Controlled Anisotropic Reinforcement Triggered by Magnetic Self-Assembly. *Macromolecules* **2011**, *44*, 8858−8865.
(35) Kim, J.; Chung, S. E.; Choi, S. E.; Lee, H.; Kim, J.; Kwon, S. Programming Magnetic Anisotropy in Polymeric Microactuators. *Nat. Mater.* **2011**, *10*, 747.
(36) Roppolo, I.; Shahzad, N.; Sacco, A.; Tresso, E.; Sangermano, M. Multifunctional NIR-Reflective and Self-Cleaning UV-Cured Coating for Solar Cell Applications Based on Cycloaliphatic Epoxy Resin. *Prog. Org. Coat.* **2014**, *77*, 458−462.
(37) Marchi, S.; Sangermano, M.; Meier, P.; Kornmann, X. Preparation and Characterization of PDMS Composites for Outdoor Polymeric Insulators. *Polym. Compos.* **2014**, *35*, 1253−1262.
(38) Matsuura, Y.; Hoshijima, J.; Ishii, R. Relation Between $Nd_2Fe_{14}B$ Grain Alignment and Coercive Force Decrease Ratio in NdFeB Sintered Magnets. *J. Magn. Magn. Mater.* **2013**, *336*, 88−92.
(39) Herbst, J. F. $R_2Fe_{14}B$ Materials: Intrinsic Properties and Technological Aspects. *Rev. Mod. Phys.* **1991**, *63*, 819−898.

DOI: 10.1021/acsami.5b04711
ACS Appl. Mater. Interfaces 2015, 7, 19112−19118